Externally-Triggered Spiking and Spiking Cluster Oscillation in Broadband Optoelectronic Oscillator

Huan Tian , Lingjie Zhang , Zhen Zeng , Yilin Wu, Zhenwei Fu, Weiqiang Lyu , Yali Zhang, Zhiyao Zhang , Shangjian Zhang , *Member, IEEE*, Heping Li , and Yong Liu

Abstract—An approach to generating periodic spiking and spiking cluster in a broadband nonlinear opto-electronic oscillator (OEO) is proposed and demonstrated. Through injecting a long-duration square-wave pulse train with a repetition frequency equal to an integral multiple of the free spectral range into the OEO with a high net gain, controllable spiking and spiking cluster oscillation can be achieved when the dual-drive Mach-Zehnder modulator (DDMZM) in the OEO is biased far away from its quadrature point. The proposed scheme is verified by both numerical simulation and experiment. The results indicate that, when the DDMZM in the OEO cavity is biased near its minimum transmission point, positive spiking train with nanosecond-level pulse width is excited by the rising edge of the injected square-wave pulse train. Through further enhancing the injection strength, uniformly-spaced positive spiking fills the high-level voltage duration of each injected square-wave pulse. Hence, spiking cluster oscillation is achieved. Benefiting from its controllability, this approach can be applied in ultra-wideband (UWB) communications, electronic countermeasures, spiking coding and high-speed neuromorphic computing.

Index Terms—Excitation, nonlinear dynamics, optoelectronic oscillator, spiking.

I. INTRODUCTION

OPTOELECTRONIC oscillators (OEOs) are self-consistent hybrid time-delay feedback oscillation systems composed of optical and electrical links. With the

Huan Tian, Lingjie Zhang, Zhen Zeng, Yilin Wu, Zhenwei Fu, and Weiqiang Lyu are with the Advanced Research Center for Microwave Photonics (ARC-MWP), School of Optoelectronic Science and Engineering, University of Electronic Science and Technology of China, Chengdu 610054, China (e-mail: huantian@std.uestc.edu.cn; zhanglingjie1993@std.uestc.edu.cn; zengzhen94@std.uestc.edu.cn; wuyilin@std.uestc.edu.cn; fuzhenwei@std.uestc.edu.cn; lyuweiqiang@std.uestc.edu.cn).

Yali Zhang, Zhiyao Zhang, Shangjian Zhang, Heping Li, and Yong Liu are with the Advanced Research Center for Microwave Photonics (ARC-MWP), School of Optoelectronic Science and Engineering, University of Electronic Science and Technology of China, Chengdu 610054, China, and also with the State Key Laboratory of Electronic Thin Films and Integrated Devices, School of Optoelectronic Science and Engineering, University of Electronic Science and Technology of China, Chengdu 610054, China (e-mail: ylzhang@uestc.edu.cn; zhangzhiyao@uestc.edu.cn; sjzhang@uestc.edu.cn; oehpli@uestc.edu.cn; yongliu@uestc.edu.cn).

assistance of narrowband filtering, OEOs working in the quasi-linear status are recognized as a promising candidate to generate microwave signals with ultra-low phase noise [1], [2], [3], [4]. In fact, the nonlinear feedback introduced by electro-optic and photoelectric conversion in a broadband OEO also leads to rich dynamic phenomena such as periodic signal, chaotic breathing and high-dimensional chaos generation [5], [6], [7], [8], [9], [10], [11]. These phenomena can be applied in chaotic encryption communication, sensing and random number generation [12], [13], [14].

Excitation is a typical nonlinear phenomenon in the feedback oscillation systems such as nonlinear circuits and injection lasers [15], [16], [17]. Based on the excitable effect, short pulses can be generated in the nonlinear oscillation systems. In the past years, excitation has also been observed in the OEOs [18], [19], [20], [21]. To realize excitation, a large and broadband net gain is essential in the OEO cavity. In addition, the Mach-Zehnder electro-optic modulator in the OEO cavity should be biased far away from its quadrature point to increase the nonlinearity and reduce the excitation threshold. In [18], multi-pulse excitability has been observed in a broadband OEO with a loop delay of 1.1 μs, which originates from the random noise in the OEO cavity. The experimental results indicate that the pulsating dynamics is repetitive on different timescales, and the irregularly distributed pulse sequences in each timescale are sensitive to the cavity parameters such as the bias voltage of the Mach-Zehnder electro-optic modulator and the net gain in the OEO loop. In [19], the oscillation initiation process of broadband chaos from random noise in an OEO under a finite-amplitude perturbation has been experimentally studied. The results show that ultra-short pulses with irregular spacing and amplitude are generated in the oscillation initiation process, which reveals that the spiking oscillation is an unstable intermediate state between the linearly stable quiescent state and the chaotic state. In [20], high-speed spiking and bursting oscillations have been experimentally demonstrated in the OEO based on a broadband microwave photonic filter, where a sinusoidal electrical control signal is used to synchronize the bursting oscillation. In the experiment, sub-nanosecond pulsating response has been achieved. Nevertheless, the spiking distribution in each spiking cluster is irregular and random. In [21], excitation of a broadband OEO under a nanosecond pulse train injection has been studied, where stable periodic spiking oscillation synchronized with the externally-injected short pulse train has been generated. This process is similar to the class II neuronal excitability, which can
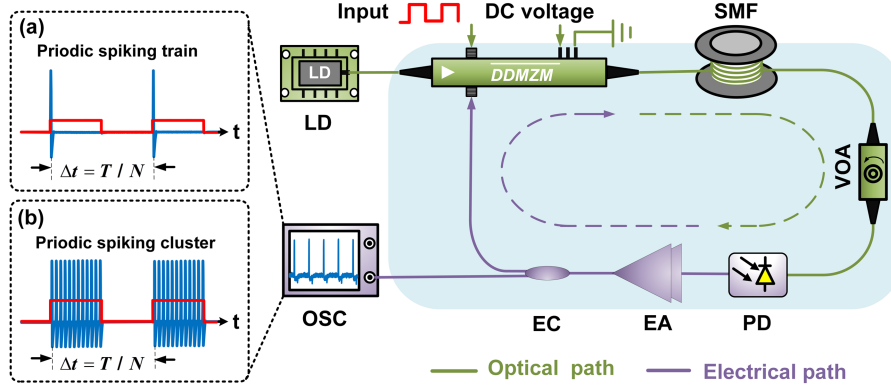
Fig. 1. Schematic diagram of the broadband OEO to realize periodic spiking and spiking cluster oscillation. T is the loop delay, and N is an integer. LD: Laser diode, DDMZM: Dual-drive Mach-Zehnder modulator, DC: Direct-current, SMF: Single-mode fiber, VOA: Variable optical attenuator, PD: Photodetector, EA: Electrical amplifier, EC: Electrical coupler, OSC: Oscilloscope.

be exploited to build optoelectronic memories, artificial neural networks and logic gates without a ruling clock.

In this paper, an approach to achieve both spiking and spiking cluster oscillation in a broadband nonlinear OEO is proposed and demonstrated. Through injecting a long-duration square-wave pulse train into the OEO cavity via a dual-drive Mach-Zehnder modulator (DDMZM), periodic spiking can be excited by the rising edge of the injected pulse, which is called the spiking oscillation state. Under strong injection, the spiking oscillation state is switched into the spiking cluster oscillation state, where uniformly-spaced spiking fills the duration of each injected pulse. To the best knowledge of the authors, it is the first time to realize controllable periodic spiking and spiking cluster oscillation in a broadband nonlinear OEO.

II. OPERATION PRINCIPLE

A. Experimental Setup

Fig. 1 shows the schematic diagram of the broadband OEO to realize periodic spiking and spiking cluster oscillation. The OEO is composed of a laser diode (LD), a high-speed DDMZM, a section of single-mode fiber (SMF), a variable optical attenuator (VOA), a high-speed photodetector (PD), a broadband electronic amplifier (EA) and a broadband electrical coupler (EC). One radio-frequency (RF) port of the DDMZM is used to close the OEO loop, and the other RF port is used to inject the long-duration square-wave pulse train into the OEO cavity. The VOA is adjusted to guarantee that the OEO cavity is with a high net gain when the DDMZM is biased at its quadrature point. In order to achieve spiking and spiking cluster oscillation, the DDMZM is biased near its minimum transmission point (MITP) to enhance the nonlinearity and reduce the excitation threshold in the OEO cavity. In addition, no filter is used in the OEO cavity. Therefore, the operation bandwidth of the OEO cavity is mainly determined by the electronic devices (especially the electrical amplifier) in the cavity, which shows a broadband characteristic. The SMF provides long-delayed feedback for the oscillation, which enriches the dynamic characteristic in the OEO cavity. Excitation can be achieved when the perturbation amplitude (i.e., the amplitude of the externally-injected square-wave pulse train)

exceeds the excitation threshold, which is described in detail below. By setting the repetition frequency of the externally-injected square-wave pulse train to be an integral multiple of the free spectral range (FSR) in the OEO loop, a periodic spiking train can be excited by the rising edge of the injected pulse train as shown in Fig. 1(a). Through further strengthening the amplitude of the injection square-wave pulse train, multiple spiking with a regular spacing can be excited in the duration of each injected pulse, which leads to periodic spiking cluster oscillation in the OEO cavity as shown in Fig. 1(b).

In the proposed scheme, spiking oscillation is formed by the combined action of the gain, the modulation nonlinearity and the broadband bandpass filtering. The open-loop voltage net gain of the OEO cavity is calculated as

$$g = \gamma G P_0 R \cos^2 \left(\frac{\pi A}{2 V_\pi} + \phi \right) \Big/ A \qquad (1)$$

where V_π is the RF half-wave voltage of the DDMZM. $\phi = \pi V_{DC}/2V_{\pi 0}$ is the phase shift of the DDMZM introduced by the direct-current (DC) bias voltage V_{DC}, in which $V_{\pi 0}$ is the DC half-wave voltage of the DDMZM. P_0 is the maximum optical power from the DDMZM. γ and R are the responsivity and the output matching resistance of the PD, respectively. G is the controllable voltage gain in the OEO loop, which is determined by the gain of the EA and the loss of the SMF, the VOA and the EC. A is the voltage amplitude of the externally-injected signal.

In fact, the broadband EA has a low cut-off frequency. Hence, the DC component of the externally-injected long-duration square-wave pulse is effectively filtered out. Only the high-frequency components at the rising and falling edges of the pulse can obtain net gain in the OEO cavity. For a periodic local perturbation, the net gain of the frequency signal is approximately calculated as

$$g_f = \gamma G P_0 R \left[\cos \left(\frac{\pi A}{V_\pi} + 2\phi \right) - \cos \left(2\phi \right) \right] \Big/ 2A \qquad (2)$$

Fig. 2(a) shows the open-loop voltage net gain curves when the DDMZM is biased near its MITP (purple line, $\phi = 0.55\pi$) and maximum transmission point (MATP, red line, $\phi = 0.95\pi$). It can be seen from Fig. 2(a) that the open-loop voltage net gain
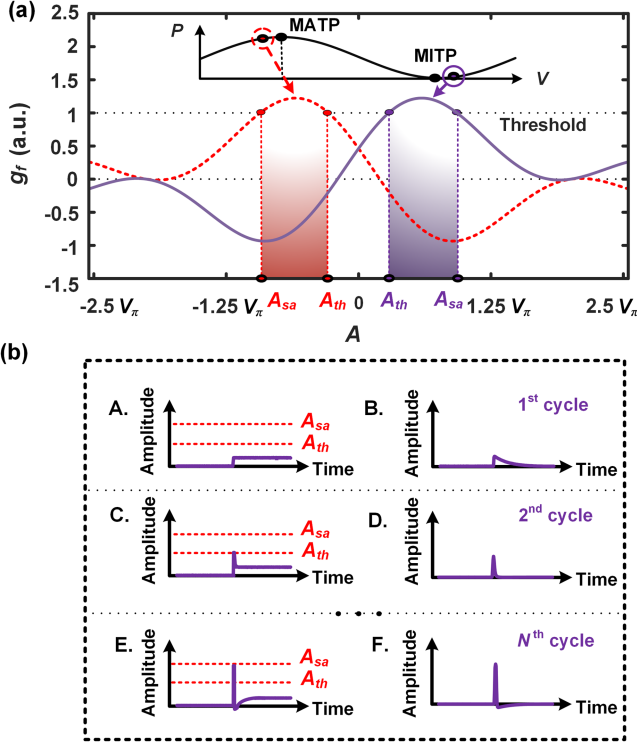
Fig. 2. Operation principle of periodic spiking oscillation by edge excitation in the broadband nonlinear OEO. A_{th} is the threshold amplitude, and A_{sa} is the saturation amplitude. (a) Open-loop voltage net gain curves when the DDMZM is biased near its MITP (purple line, $\phi=0.55\pi$) and MATP (red line, $\phi=0.95\pi$). (b) Periodic spiking generation process under a weak long-duration square-wave pulse train injection.

increases with the perturbation amplitude (i.e., the amplitude of the externally-injected pulse train) for the DDMZM biased near its MITP. When the perturbation amplitude exceeds the threshold A_{th}, the rising edge of the injected pulse will be strengthened in the closed OEO cavity since $g_f > 1$. It finally trends to saturation when its amplitude reaches the saturation amplitude A_{sa}. Fig. 2(b) shows the excitation process under a weak long-duration square-wave pulse train injection. The rising edge of the injected long-duration square-wave pulse is shown as inset A of Fig. 2(b), After electro-optic modulation in the DDMZM, photoelectric conversion in the PD and the high-pass filtering effect in the EA, the rising edge of the long-duration square-wave pulse will be shaped to a sharp residual waveform as shown in the inset B of Fig. 2(b). Then, it overlaps with the next externally-injected square-wave pulse as shown in the inset C of Fig. 2(b). If the peak of the overlapped waveform exceeds the threshold A_{th}, it will be amplified in the OEO cavity, while the other components are filtered out again. Hence, a sharp spiking as shown in the inset D of Fig. 2(d) is generated in the OEO cavity. After multiple circulation in the OEO cavity, the amplitude of the spiking gradually increases as shown in the inset E of Fig. 2(b). When the spiking amplitude reaches A_{sa}, as shown in the inset F of Fig. 2(b), a stable periodic spiking train synchronized with the externally-injected long-duration square-wave pulse train is generated. If the injection strength is further increased, the tail of the overlapped waveform as shown in the
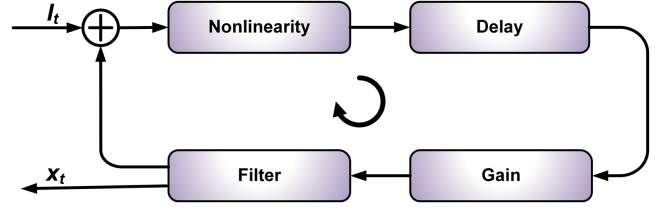
inset E of Fig. 2(b) will be enhanced to excite more spiking in the duration of the externally-injected long-duration square-wave pulse. Hence, a stable periodic spiking cluster synchronized with the externally-injected long-duration square-wave pulse train is generated in the OEO cavity. It should be pointed out that periodic spiking and spiking cluster can also be generated when the DDMZM is biased near its MATP. The only difference is that the generated spiking and spiking cluster are with negative voltages.

B. Theoretical Model

Fig. 3 presents the theoretical model of the broadband nonlinear OEO, which includes the cosine-squared nonlinearity induced by the MZM and the PD, the time delay of the OEO loop, the linear broadband bandpass filtering induced by the devices in the cavity, the net gain and the injection perturbation.

For simplicity, the bandpass filtering effect in the OEO cavity is modeled as a 2nd-order linear bandpass filter (BPF) with a low cut-off frequency of f_L and a high cut-off frequency of f_H. Therefore, the dynamic process in the OEO can be mathematically described as

$$\left(1 + \frac{\tau}{\theta}\right) x_t + \tau \frac{dx_t}{dt} + \frac{1}{\theta} \int_{t_0}^t x_t dt = \beta \cos^2 \left(x_{t-T} + I_t + \phi\right) \tag{3}$$

where $x_t = \pi V_t / 2V_\pi$ is the dimensionless variable of the microwave signal V_t in the OEO cavity. τ and θ are the characteristic time of the BPF, which are inversely proportional to f_H and f_L, respectively. T is the loop delay. $\beta = \gamma G P_0 R \pi / 2V_\pi$ is the gain coefficient. I_t denotes the injected square wave with a repetition frequency equal to an integral multiple of the FSR (i.e., the reciprocal of the loop delay) in the OEO cavity. By defining an integral term as

$$y_t = \frac{1}{\theta} \int_{t_0}^t x_t dt \tag{4}$$

Equation (3) can be rewritten as

$$\frac{dx_t}{dt} = -\left(\frac{1}{\tau} + \frac{1}{\theta}\right) x_t - \frac{y_t}{\tau} + \frac{\beta}{\tau} \cos^2 \left(x_{t-T} + I_t + \phi\right)$$

$$\frac{dy_t}{dt} = \frac{x_t}{\theta} \tag{5}$$

When there is no injection signal (i.e., $I_t = 0$), (5) is a typical modified Ikeda-like equation, whose stability is mainly affected by the bias voltage and the loop gain, and there is only one fixed point of $(0, \beta \cos^2(\phi))$ for this dynamic equation. If the

Fig. 3. Theory model of the proposed broadband nonlinear OEO.

gain coefficient in the OEO reaches a critical value, the dynamic system enters a self-starting oscillation state from noise through Hopf bifurcation. The gain coefficient threshold to realize Hopf bifurcation can be numerically calculated based on (5) by using the linearization theory as

$$\beta_H \approx 1/\sin(2\phi) \tag{6}$$

It can be seen from (6) that, when the DDMZM is biased near its linear transmission point (i.e., $\phi = \pi/4$), the gain coefficient threshold is the lowest (i.e., $\beta_H = 1$) that a stable limit cycle oscillation can be easily established in the OEO. The limit cycle oscillation corresponds to the trajectory determined in the phase space and the frequency solution of (5). Nevertheless, this situation changes as the bias voltage of the DDMZM approaches the MITP or the MATP. When the DDMZM is biased at the MITP (i.e., $\phi = \pi/2$) or the MATP (i.e., $\phi = \pi$), the bifurcation threshold increases to infinity so that no limit cycle oscillation can be established in the OEO from the noise. On this condition, for any small perturbation introduced by the externally-injected signal, it is asymptotically stable with the evolution of the dynamic system. Hence, excitation can be achieved, where a voltage jumping perturbation exceeding the A_{th} in the time domain can be shaped as a spiking under the balance of the nonlinearity and the bandpass filtering effect.

In order to better describe the dynamic process of excitation, the nullclines corresponding to the curves with a partial derivative of zero is used to characterize the trajectory of the excited spiking, which can be derived from (5) as

$$\begin{cases} y_t = -\left(1 + \frac{\tau}{\theta}\right)x_t + \beta\cos^2(x_{t-T} + \phi) \\ x_t = 0 \end{cases} \tag{7}$$

Assisted with the nullclines in (7) and its corresponding partial derivative in (5), the dynamic process and the evolution direction in the phase portrait can be clearly characterized. Moreover, in order to reduce the computational complexity and accelerate the converge to the stable oscillation state, the pulse tracking method in [25] is used to numerically solve (3), where the filtering process is calculated in the frequency domain by carrying out fast Fourier transform (FFT), and the nonlinearity is calculated in the time domain.

III. SIMULATION RESULTS

In the numerical simulation, the loop delay is set to be $T = 1018$ ns, which corresponds to a spool of SMF with a length of 200 m. The transmission loss coefficient of the SMF is 0.2 dB/km at 1550 nm. The optical power from the LD at 1550 nm is 16 dBm. The DDMZM is with a fiber-to-fiber insertion loss of 3 dB, an RF half-wave voltage of $V_\pi = 4$ V, a DC half-wave voltage of $V_{\pi0} = 4$ V and a DC bias voltage of 4.2 V. These parameter settings guarantee that the DDMZM is working near its MITP (i.e., $\phi = 0.525\pi$). In addition, the low cut-off frequency f_L and the high cut-off frequency f_H of the 2nd-order BPF are set to be 31.83 MHz and 3.18 GHz, respectively. The responsivity and the output matching resistance of the PD are 0.8 A/W and 50 Ω, respectively. In addition, an initial white noise with a power

spectral density of -160 dBm/Hz is added to each circulation in the OEO cavity.

A. Spiking Oscillation

In order to achieve spiking oscillation, the period of the externally-injected square-wave pulse train is set to be 1018 ns, which is equal to the loop delay of the OEO. Each square-wave pulse is with a duration of 509 ns, a rising/falling time of 5 ns, a high-level voltage of 0.35 V and a low-level voltage of 0 V. The gain coefficient is set to be $\beta = 1.4804$. Fig. 4(a) and (b) exhibit the dynamic evolution process of the phase portrait and the temporal waveform in the broadband OEO. In Fig. 4(a), the blue solid line, the red dashed line and the red arrows represent the phase trajectory, the nullclines and the evolution directions, respectively. In the dashed box of Fig. 4(b), the temporal waveforms after 20, 50 and 100 circles are presented, where the blue solid line and the red dashed line denote the temporal waveform of the spiking and the injected square-wave pulse, respectively. It can be seen from Fig. 4(b) that the injected square-wave pulse provides the initial spiking instead of the noise in the OEO cavity. The amplitude of the spiking increases with the circulation number. After 50 cycles, strong spiking is generated through excitation, whose pulse width is then enlarged due to the combined influence of the gain, the bandpass filtering effect and the nonlinearity in the OEO cavity. Especially, the broadband bandpass filtering prevents further temporal expansion of the generated spiking after 100 cycles. Hence, stable spiking oscillation is excited by the rising edge of the injected square-wave pulse as shown in Fig. 4(b). Correspondingly, it can be seen from Fig. 4(a) that the OEO deviates from the equilibrium point at $x = 0$ and $y = 0$, and walks a circle along the direction of the red arrows after a single circulation. At the early stage of the oscillation, the range of the phase trajectory expands with the circulation number. Then, it saturates as the generated spiking reach a stable status.

Fig. 5 shows the simulation results under stable spiking oscillation. It can be seen from Fig. 5(a) that the rising edge of each injected square-wave pulse excites a positive spiking in the OEO cavity. Nevertheless, the falling edge of each injected square-wave pulse cannot obtain enough gain, and forms a residual small negative spiking. The unwanted residual spiking can be suppressed by using an injected waveform with a gradual falling edge, e.g., a sawtooth waveform. The generated positive spiking is with a pulse width of 1.4 ns as depicted in Fig. 5(b). It is also shown in Fig. 5(b) that the generated positive spiking is with a long negative tail, which corresponds to the slow time scale of the phase trajectory defined by the dynamic equation, and is similar to the characteristic of the class II optical neurons. In Fig. 5(c), the red line and the blue line represent the dimensionless waveform x and its integral value y, respectively. It should be noted that the integration curve restores the envelope of the injected square-wave pulse, where each rising edge contains a spiking. Based on the calculated x and y, the phase portrait under stable spiking oscillation is exhibited in Fig. 5(d), where the points A, B, C, D, E and F
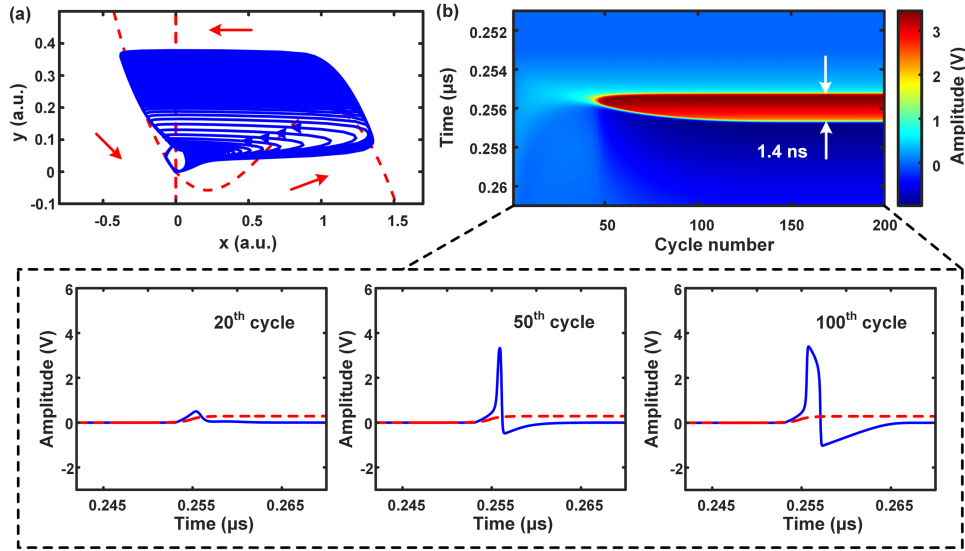
Fig. 4. Dynamic evolution process in the broadband OEO under spiking oscillation. (a) Phase portrait. The blue solid line, the red dashed line and the red arrows represent the phase trajectory, the nullclines and the evolution direction, respectively. (b) Temporal waveform evolution. The blue solid line and the red dashed line in the dashed box denote the temporal waveforms of the generated spiking and the injected square-wave pulse, respectively.
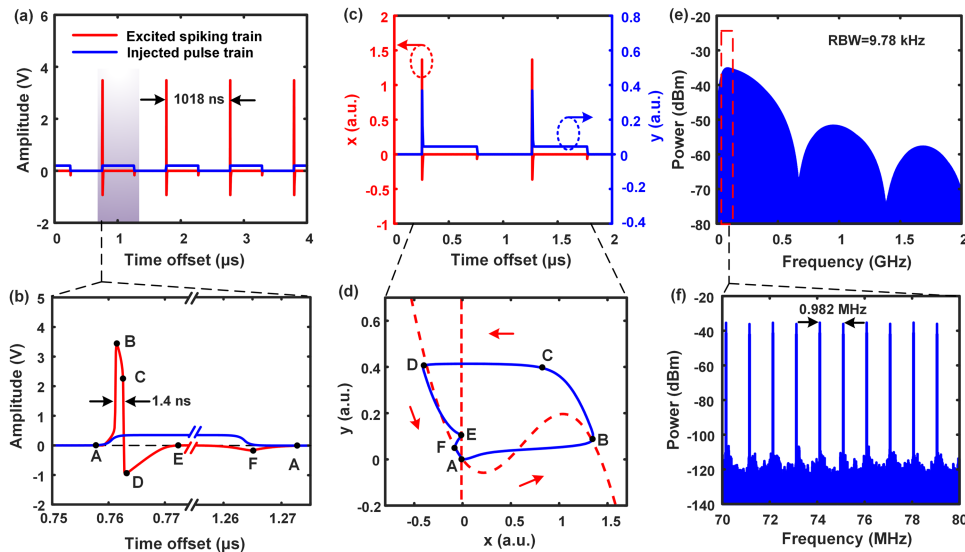

Fig. 5. Simulation results under stable spiking oscillation. (a) Temporal waveforms of the generated spiking train (red line) and the injected pulse train (blue line). (b) Temporal waveform details of the generated spiking train (red line) and the injected pulse train (blue line). (c) Temporal waveform of the generated spiking train (red line) and its integral characteristic (blue line) involving two periods. (d) Phase portrait evolution in two periods. The blue solid line, the red dashed line and the red arrows represent the phase trajectory, the nullclines and the evolution direction, respectively. (e) Spectrum of the generated spiking train. (f) Spectrum detail of the generated spiking train.

correspond to those in Fig. 5(b), respectively. It can be seen from Fig. 5(c) and (d) that the dynamic evolution returns to the equilibrium point A, i.e., $x = 0$ and $y = 0$, only after the residual negative spiking in each period. These results indicate that the dynamic evolution characteristic of the spiking oscillation is determined by both the spiking phase trajectory generated by the rising edge excitation and the differential waveform of the injected square-wave pulse. In addition, Fig. 5(e) and (f) present the spectrum and the spectrum detail of the generated spiking train, respectively, which are obtained by implementing FFT of

the waveforms within a time window of 101.8 μs. The spectrum is with an envelope analogue to the sinc function except for the power degradation at the low-frequency band near the DC induced by the high-pass filtering effect in the OEO cavity. The mode interval is 0.982 MHz, which is equal to the FSR of the OEO cavity.

Fig. 6 presents the simulation results under stable spiking oscillation, where the period of the externally-injected square-wave pulse train is reduced to 509 ns, and the duty cycle is maintained to be 50%. It can be seen from Fig. 6(a) that a spiking train
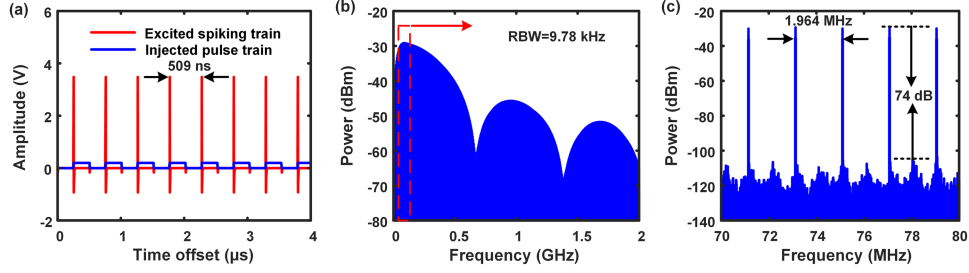
Fig. 6. Simulation results under stable spiking oscillation when the period of the externally-injected square-wave pulse train is set to be 509 ns. (a) Temporal waveforms of the generated spiking train (red line) and the injected pulse train (blue line). (b) Spectrum of the generated spiking train. (c) Spectrum detail of the generated spiking train.
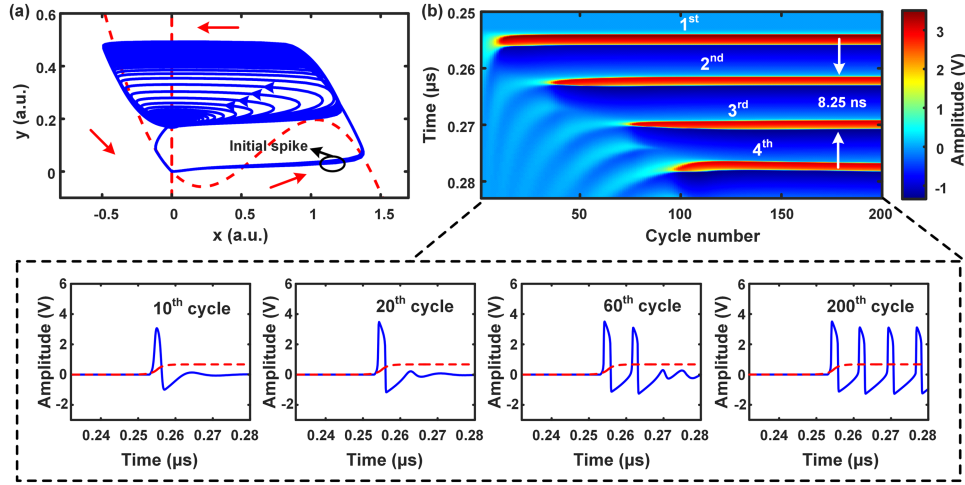

Fig. 7. Dynamic evolution process in the broadband OEO under spiking cluster oscillation. (a) Phase portrait from the 20th cycle to the 60th cycle. The blue solid line, the red dashed line and the red arrows represent the phase trajectory, the nullclines and the evolution direction, respectively. (b) Temporal waveform evolution. The blue solid line and the red dashed line in the dashed box denote the temporal waveforms of the generated spiking and the injected square-wave pulse, respectively.

with an interval of 509 ns, i.e., a repetition frequency of 1.964 MHz, is successfully excited in the OEO cavity by the rising edge of each injected square-wave pulse, which is similar to the 2nd-order harmonic mode locking. The supermode suppression ratio is 74 dB as depicted in Fig. 6(c), which indicates that the generated spiking train is with an excellent pulse-to-pulse consistency. Through further setting the repetition frequency of the externally-injected square-wave pulse train to be N times of the FSR in the OEO cavity ($N \geq 3$), spiking trains synchronized with the injected square-wave pulse train can be generated by the rising edge excitation, which is similar to the Nth-order harmonic mode locking.

It should be pointed out that, through biasing the DDMZM near its MATP, negative spiking trains can also be generated in the broadband OEO. Compared with the random spiking oscillation in a self-starting long-delayed broadband OEO, the spiking train excited by the externally-injected square-wave pulse train shows an excellent controllability. In addition, through further increasing the low cut-off frequency f_L, spiking trains with pulse widths in the sub-nanosecond level can be excited in the OEO.

B. Spiking Cluster Oscillation

In order to achieve spiking cluster oscillation, the high-level voltage of the externally-injected square-wave pulse train used in Fig. 4 is increased to 0.60 V. The gain coefficient is also set to be $\beta = 1.4804$. Fig. 7 shows the dynamic evolution process in the broadband OEO, where Fig. 7(a) exhibits the phase portrait from the 20th cycle to the 60th cycle. It can be seen from Fig. 7(b) that the initial spiking is stably formed after 20 cycles, where its build-up time is reduced compared with that in Fig. 4 due to the enhancement of injection strength. After the initial spiking reaches stability in the 20th cycle, another small spiking begins to rise up till it reaches saturation, which forms the second spiking as depicted by the phase portrait in Fig. 7(a) and the middle two Figures in the dashed box of Fig. 7(b). Subsequently, multiple spiking with an identical interval is excited in sequence, which gradually fill the duration of the high-level voltage as shown in Fig. 7(b).

Fig. 8 shows the simulation results under stable spiking cluster oscillation. It can be seen from Fig. 8(a) and (b) that a uniformly-spaced spiking cluster with a spiking interval of 8.25
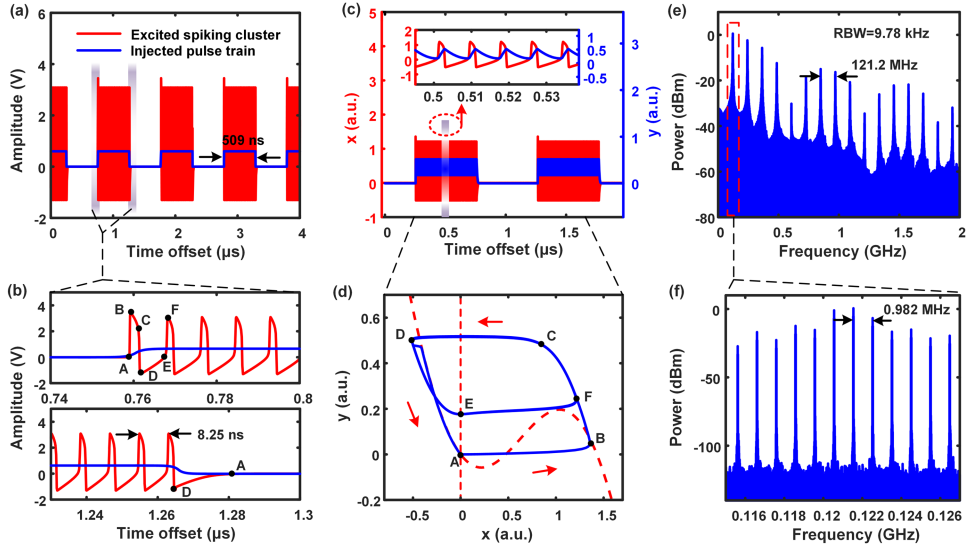
Fig. 8. Simulation results under stable spiking cluster oscillation. (a) Temporal waveforms of the generated spiking clusters (red line) and the injected pulse train (blue line), (b) Temporal waveform details of the generated spiking cluster train (red line) and the injected pulse train (blue line). (c) Temporal waveform of the generated spiking cluster train (red line) and its integral characteristic (blue line) involving two periods. (d) Phase portrait evolution in two periods. The blue solid line, the red dashed line and the red arrows represent the phase trajectory, the nullclines and the evolution direction, respectively. (e) Spectrum of the generated spiking cluster train. (f) Spectrum detail of the generated spiking cluster train.
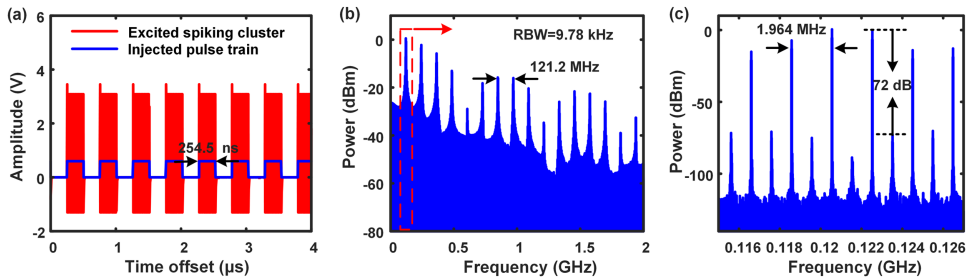

Fig. 9. Simulation results under stable spiking cluster oscillation when the period of the externally-injected square-wave pulse train is set to be 509 ns. (a) Temporal waveforms of the generated spiking train (red line) and the injected pulse train (blue line). (b) Spectrum of the generated spiking train. (c) Spectrum detail of the generated spiking train.

ns fills the high-level voltage duration of each injected square-wave pulse. Correspondingly, the interval of the neighboring frequency cluster is equal to 121.2 MHz as shown in Fig. 8(e). For each frequency cluster as depicted in Fig. 8(f), the interval of the neighboring frequency component is 0.982 MHz, which is equal to the FSR of the OEO cavity. In Fig. 8(c), the red line and the blue line represent the dimensionless waveform x and its integral value y, respectively. Based on the calculated x and y, the phase portrait under stable spiking cluster oscillation is exhibited in Fig. 8(d), where the points A, B, C, D, E and F correspond to those in Fig. 8(b), respectively. It can be seen that the phase trajectory in Fig. 8(d) is different from that in Fig. 5(d). In each spiking cluster, the phase trajectory forms a new cycle through points C, D, E and F from spiking to spiking, which returns to the equilibrium point A only at the end of the spiking cluster.

Fig. 9 shows the simulation results under stable spiking cluster oscillation, where the period of the externally-injected square-wave pulse train is reduced to 509 ns, and the duty cycle

is maintained to be 50%. It can be seen from Fig. 9(b) that the interval of the neighboring frequency cluster is 121.2 MHz, which indicates that the time interval of the neighboring spiking in each spiking cluster is identical to that in Fig. 8(b). In addition, the supermode suppression ratio is 72 dB as depicted in Fig. 9(c), which indicates that the generated periodic spiking cluster is with an excellent cluster-to-cluster coherence.

It should be pointed out that, through biasing the DDMZM near its MATP, negative spiking cluster trains can also be generated in the broadband OEO. The pulse width of each spiking and the spiking interval in a spiking cluster are closely related to the dynamic parameters. Through further increasing the low cut-off frequency f_L, both the pulse width and the spiking interval in a spiking cluster can be reduced.

Finally, it should be pointed out that the parameters of the generated spiking and spiking cluster sequence can be tuned by varying the externally-injected signal. For example, through varying the duty cycle of the externally-injected square-wave pulse train, the duration of the generated spiking cluster varies
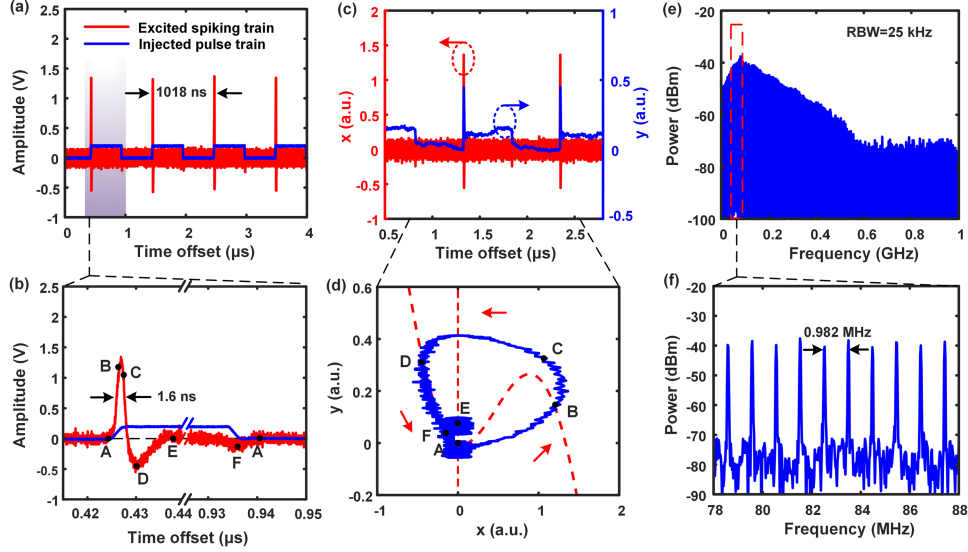
Fig. 10. Experimental results under stable spiking oscillation. (a) Temporal waveform of the generated spiking train (red line) and the injected pulse train (blue line). (b) Temporal waveform details of the generated spiking train (red line) and the injected pulse train (blue line). (c) Temporal waveform of the generated spiking train (red line) and its integral characteristic (blue line) involving two periods. (d) Phase portrait evolution in two periods. The blue solid line, the red dashed line and the red arrows represent the phase trajectory, the nullclines and the evolution direction, respectively. (e) Spectrum of the generated spiking train. (f) Spectrum detail of the generated spiking train.

correspondingly. Through injecting an on-off keying (OOK) coded square-wave pulse train with a repetition frequency equal to an integral multiple of the FSR into the OEO cavity, either a spiking sequence or a spiking cluster sequence with the corresponding OOK code and repetition frequency can be generated. Through injecting a square-wave pulse train with a repetition frequency equal to 1/N of the FSR into the OEO cavity, a spiking sequence can also be generated. In summary, the most prominent characteristic of the proposed OEO scheme lies in that the generated spiking and spiking cluster are triggered by the externally-injected signal. Hence, compared with the random spiking oscillation built from noise in [19], the spiking and spiking cluster generation by using the proposed scheme is controllable.

IV. EXPERIMENTAL RESULTS

A proof-of-concept experiment is carried out to verify the feasibility of the proposed scheme to generate controllable spiking and spiking cluster oscillation. The continuous-wave optical carrier for the broadband nonlinear OEO is generated by using a high-power distributed feedback laser diode (DFB-LD), where the center wavelength and the output power are 1548.9 nm and 15.6 dBm, respectively. The DDMZM (EOSPACE AE-DD-0VPP-40-PFA-SFA) is biased near its MITP, where the bias voltage for the MITP and the applied DC bias voltage are 4 V and 4.2 V, respectively. The externally-injected square-wave pulse train is generated by using an arbitrary waveform generator (RIGOL DG5352) with a sampling rate of 1 GSa/s and a maximum output frequency of 350 MHz. The SMF in the cavity is with a length of 200 m. A hand-driven VOA is employed to adjust the optical power injected into the PD (HP 11982A). An LNA (GT-HLNA-0022G) with an operation bandwidth from

34.25 MHz to 22 GHz and a small-signal gain of 28 dB is used to amplify the signal from the PD. An electrical power divider (GTPD-COMB50G) with an operation bandwidth from DC to 50 GHz is used to extract the signal out of the OEO cavity. The loop delay of the OEO cavity is measured to be 1018 ns. The waveforms of the generated periodic spiking and spiking cluster are recorded by using a high-speed oscilloscope (Tektronix DPO75002SX) with a sampling rate of 50 GSa/s. In addition, the spectrum of the generated signal is obtained by implementing FFT of the waveforms.

A. Spiking Oscillation

The injected square-wave pulse train is set to be with a period of 1018 ns and a duty cycle of 50%. Thereinto, each square-wave pulse is with a rising time/falling time of 3.9 ns, a high-level voltage of 0.2 V and a low-level voltage of 0 V. The loop gain is tuned through the VOA. When the loop gain is small, it is observed that the OEO cavity keeps in a stable state (i.e., $x = 0$, $y = 0$). Through tuning the loop gain beyond the excitation threshold, stable spiking oscillation is formed by the rising-edge excitation. Fig. 10(a)–(f) show the temporal waveform, the waveform detail, the integral value y, the phase portrait, the spectrum and the spectrum detail of the generated spiking train under stable oscillation, respectively. It can be seen from Fig. 10(a) and (b) that the generated positive spiking train is with a spiking interval of 1018 ns and a pulse width of 1.6 ns, respectively, which fit in with the simulation results in Fig. 5. The only difference is that the positive spiking obtained in the experiment is more symmetrical than that obtained by the numerical simulation. Hence, the spectrum envelope in Fig. 10(e) is smoother than that in Fig. 5(e). The closed phase trajectory in Fig. 10(d) is identical to that in Fig. 5(d) except for the relatively
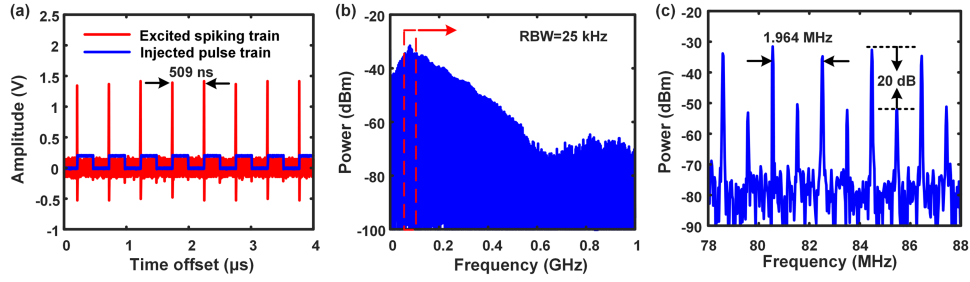
Fig. 11.   Experimental results under stable spiking oscillation when the period of the externally-injected square-wave pulse train is set to be 509 ns. (a) Temporal waveforms of the generated spiking train (red line) and the injected pulse train (blue line). (b) Spectrum of the generated spiking train. (c) Spectrum detail of the generated spiking train.
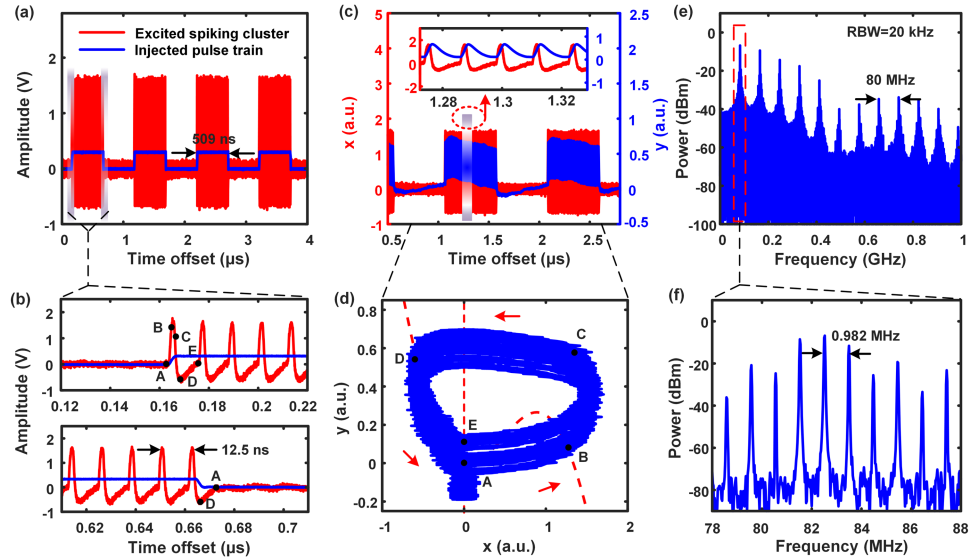

Fig. 12.   Experimental results under stable spiking cluster oscillation. (a) Temporal waveforms of the generated spiking clusters (red line) and the injected pulse train (blue line), (b) Temporal waveform details of the generated spiking cluster train (red line) and the injected pulse train (blue line). (c) Temporal waveform of the generated spiking cluster train (red line) and its integral characteristic (blue line) involving two periods. (d) Phase portrait evolution in two periods. The blue solid line, the red dashed line and the red arrows represent the phase trajectory, the nullclines and the evolution direction, respectively. (e) Spectrum of the generated spiking cluster train. (f) Spectrum detail of the generated spiking cluster train.

large noise, indicating that global stability is maintained in each spiking period.

Fig. 11 shows the experimental results under stable spiking oscillation, where the period of the externally-injected square-wave pulse train is reduced to be 509 ns, and the duty cycle is maintained to be 50%. It can be seen that these results fit in with the simulation results in Fig. 6 except for the spectrum envelope and the supermode suppression ratio. The relatively low supermode suppression ratio of only 20 dB in the experiment is mainly attributed to the mismatching between the period of the injected square-wave pulse train and the loop delay. In addition, the dispersion introduced by the SMF and the electronic devices in the OEO cavity also contributes to the deterioration of the supermode suppression ratio. Hence, the supermode suppression ratio can be improved by inserting an optical tunable delay line with a high-precision tuning step into the OEO cavity to finely tune the FSR. In addition, a DFB-LD at 1310 nm is beneficial for reducing the intra-cavity dispersion of the OEO introduced by the SMF.

B. Spiking Cluster Oscillation

Spiking cluster oscillation is obtained by increasing the high-level voltage of the externally-injected square-wave pulse train used in Fig. 10 to 0.30 V. Fig. 12(a)–(f) show the temporal waveform, the waveform detail, the integral value y, the phase portrait, the spectrum and the spectrum detail of the generated spiking cluster train under stable oscillation, respectively. It can be seen from Fig. 12(a) and (b) that stable spiking cluster oscillation is successfully built, where uniformly-spaced spiking cluster with a nanosecond-level pulse width and a spiking interval of 12.5 ns fills the high-level voltage duration of each injected long square-wave pulse. Correspondingly, the interval of the neighboring frequency cluster is equal to 80 MHz as shown in Fig. 12(e). The increase of the spiking interval in the experiment compared with that in Fig. 8 is mainly attributed to that the actual frequency response of the OEO cavity is different from that of the 2nd-order BPF used in the simulation. Especially, the low cut-off frequency f_L is smaller than that in the simulation. In addition,
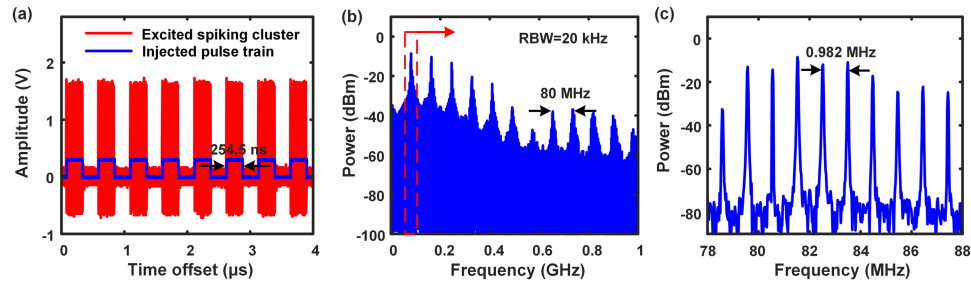
Fig. 13. Experimental results under stable spiking cluster oscillation when the period of the externally-injected square-wave pulse train is set to be 509 ns. (a) Temporal waveforms of the generated spiking train (red line) and the injected pulse train (blue line). (b) Spectrum of the generated spiking train. (c) Spectrum detail of the generated spiking train.

the high-level voltage of the injected square-wave pulse train is much smaller than that in the simulation. This also contributes to the increase of the spiking interval in the experiment. Although the nested double ring of the phase portrait in Fig. 12(d) is not as clear as that in Fig. 8(d), its closed-loop characteristic still indicates that stable limit cycle oscillation is established among cycles.

Fig. 13 shows the experimental results under stable spiking cluster oscillation, where the repetition period of the externally-injected square-wave pulse train is reduced to 509 ns, and the duty cycle is maintained to be 50%. It can be seen from Fig. 13(b) that the interval of the neighboring frequency cluster is equal to that in Fig. 12, indicating that the decrease of the period has no influence on the spiking interval in each spiking cluster. In addition, the supermode noise in Fig. 13(c) is strong, which is attributed to the mismatching between the period of the injected square-wave pulse train and the loop delay. The weak supermode suppression ratio indicates that the cluster-to-cluster coherence in the experiment is worse than that in the simulation, which can be improved by increasing the synchronization accuracy of the externally-injected signal.

V. CONCLUSION

In summary, we have proposed and demonstrated an approach to achieving controllable spiking and spiking cluster oscillation in a broadband nonlinear OEO by injecting a long-duration square-wave pulse train into the cavity. To achieve stable oscillation, the repetition frequency of the externally-injected square-wave pulse train must be equal to an integral multiple of the FSR into the OEO cavity, and the OEO cavity must have a high net gain. When the DDMZM is biased near its MITP, positive spiking train with nanosecond-level pulse width is excited by the rising edge of the injected signal. Through further enhancing the injection strength, uniformly- spaced positive spiking fills the high-level voltage duration of each injected square-wave pulse. Therefore, spiking cluster oscillation is achieved. The proposed scheme is verified by both numerical simulation and experiment, where the experimental results fit in with the simulation results. In addition, negative spiking train and spiking cluster train can also be excited through biasing the DDMZM near its MATP. The proposed scheme can be applied in ultra-wideband (UWB) communications, electronic countermeasures and high-speed neuromorphic calculation.

REFERENCES

[1] M. Li, T. F. Hao, W. Li, and Y. T. Dai, "Tutorial on optoelectronic oscillators," *APL Photon.*, vol. 6, no. 6, Jun. 2021, Art. no. 061101.

[2] T. F. Hao et al., "Recent advances in optoelectronic oscillators," *Adv. Photon.*, vol. 2, no. 4, Jul. 2020, Art. no. 044001.

[3] L. Malaki, "The optoelectronic oscillator," *Nature Photon.*, vol. 5, no. 12, pp. 728–730, Dec. 2011.

[4] A. Liu, J. Dai, and K. Xu, "Stable and low-spurs optoelectronic oscillators: A review," *Appl. Sci.*, vol. 8, no. 12, Dec. 2018, Art. no. 2623.

[5] J. H. T. Mbé, P. Woafo, and Y. K. Chembo, "A normal form method for the determination of oscillations characteristics near the primary Hopf bifurcation in bandpass optoelectronic oscillators: Theory and experiment," *Chaos*, vol. 29, no. 3, Mar. 2019, Art. no. 033104.

[6] Y. Xiao, Y. T. Dai, N. N. Shi, W. Li, N. H. Zhu, and M. Li, "Microwave-photonics iterative nonlinear gain model for optoelectronics oscillators," *Opt. Exp.*, vol. 30, no. 7, pp. 12131–12149, Mar. 2022.

[7] N. Li and J. Wei, "Bifurcation analysis in a nonlinear electro-optical oscillator with delayed bandpass feedback," *Nonlinear Dyn.*, vol. 96, no. 1, pp. 483–496, Apr. 2019.

[8] G. R. G. Chengui et al., "Theoretical and experimental study of slow-scale Hopf limit-cycles in laser-based wideband optoelectronic oscillators," *J. Opt. Soc. Amer. B*, vol. 31, no. 10, pp. 2310–2316, Oct. 2014.

[9] Y. C. Kouomou, P. Colet, L. Larger, and N. Gastaud, "Chaotic breathers in delayed electro-optical systems," *Phys. Rev. Lett.*, vol. 95, no. 20, Nov. 2005, Art. no. 203903.

[10] B. Romeira, F. Q. Kong, W. Z. Li, J. M. L. Figueiredo, J. Javaloyesl, and J. P. Yao, "Broadband chaotic signals and breather oscillations in an optoelectronic oscillator incorporating a microwave photonic filter," *J. Lightw. Technol.*, vol. 32, no. 20, pp. 3933–3942, Oct. 2014.

[11] R. Lavrov, M. Peil, L. Larger, V. Udaltsov, and J. Dudley, "Electro-optic delay oscillator with nonlocal nonlinearity: Optical phase dynamics, chaos, and synchronization," *Phys. Rev. E*, vol. 80, no. 2, Aug. 2009, Art. no. 026207.

[12] Y. K. Chembo, D. Brunner, M. Jacquot, and L. Larger, "Optoelectronic oscillators with time-delayed feedback," *Rev. Modern Phys.*, vol. 91, no. 3, Sep. 2019, Art. no. 035006.

[13] F. Böhm, S. Sahakian, A. Dooms, G. Verschaffelt, and G. V. Sande, "Stable high-speed encryption key distribution via synchronization of chaotic optoelectronic oscillators," *Phys. Rev. Appl.*, vol. 13, no. 6, Jun. 2020, Art. no. 064014.

[14] P. H. Mu, W. Pan, S. Y. Xiang, N. Q. Li, X. K. Liu, and X. H. Zou, "Fast physical and pseudo random number generation based on a nonlinear optoelectronic oscillator," *Modern Phys. Lett. B*, vol. 29, no. 24, Sep. 2015, Art. no. 1550142.

[15] S. Barbay, R. Kuszelewicz, and A. M. Yacomotti, "Excitability in a semiconductor laser with saturable absorber," *Opt. Lett.*, vol. 36, no. 5, pp. 4476–4478, Dec. 2011.

[16] W. T. Prants and C. Bonatto, "Triple point of synchronization, phase singularity, and excitability along the transition between unbounded and bounded phase oscillations in a forced nonlinear oscillator," *Phys. Rev. E*, vol. 103, no. 3, Mar. 2021, Art. no. 032201.

[17] Y. H. Zhang, S. Y. Xiang, J. K. Gong, X. X. Guo, A. J. Wen, and Y. Hao, "Spike encoding and storage properties in mutually coupled vertical-cavity surface-emitting lasers subject to optical pulse injection," *Appl. Opt.*, vol. 57, no. 7, pp. 1731–1737, Mar. 2018.

[18] M. Peil, M. Jacquot, Y. K. Chembo, L. Larger, and T. Erneux, "Routes to chaos and multiple time scale dynamics in broadband bandpass nonlinear delay electro-optic oscillators," *Phys. Rev. E*, vol. 79, no. 2, Feb. 2009, Art. no. 026208.

[19] K. E. Callan, L. Illing, Z. Gao, D. J. Gauthier, and E. Schöll, "Broadband chaos generated by an optoelectronic oscillator," *Phys. Rev. Lett.*, vol. 104, no. 11, Mar. 2010, Art. no. 113901.

[20] B. Romeira, F. Q. Kong, J. M. L. Figueiredo, J. Javaloyes, and J. P. Yao, "High-speed spiking and bursting oscillations in a long-delayed broadband optoelectronic oscillator," *J. Lightw. Technol.*, vol. 33, no. 2, pp. 503–510, Jan. 2015.

[21] D. P. Rosin, K. E. Callan, D. J. Gauthier, and E. Scholl, "Pulse-train solutions and excitability in an optoelectronic oscillator," *Europhysics Let.*, vol. 96, no. 3, Nov. 2011, Art. no. 34001.

[22] S. Y. Xiang, Z. X. Ren, Y. H. Zhang, Z. W. Song, and Y. Hao, "All-optical neuromorphic XOR operation with inhibitory dynamics of a single photonic spiking neuron based on a VCSEL-SA," *Opt. Lett.*, vol. 45, no. 5, pp. 1104–1107, Mar. 2020.

[23] R. Wang, C. Qian, Q. S. Ren, and J. Y. Zhao, "Optoelectronic neuromorphic system using the neural engineering framework," *Appl. Opt.*, vol. 56, no. 5, pp. 1517–1525, Feb. 2017.

[24] J. Robertson, T. Deng, J. Javaloyes, and A. Hurtado, "Controlled inhibition of spiking dynamics in VCSELs for neuromorphic photonics: Theory and experiments," *Opt. Lett.*, vol. 42, no. 8, pp. 1560–1563, Apr. 2017.

[25] Y. L. Wu et al., "Modeling an actively mode-locked optoelectronic oscillator based on electric amplitude modulation," *Opt. Exp.*, vol. 29, no. 15, pp. 23835–23846, Jul. 2021.

Huan Tian received the B.S. degree from the Wuhan University of Technology, Wuhan, China, in 2019. He is currently working toward the Ph.D. degree with the School of Optoelectronic Science and Engineering, University of Electronic Science and Technology of China, Chengdu, China. His research interests include optoelectronic oscillator and nonlinear dynamics.

Lingjie Zhang received the B.S. degree in 2016 from the University of Electronic Science and Technology of China, Chengdu, China, where he is currently working toward the Ph.D. degree with the School of Optoelectronic Science and Engineering. His research interests include mode-locking optoelectronic oscillator and microwave photonic radar.

Zhen Zeng received the B.S. degree in 2016 from the University of Electronic Science and Technology of China, Chengdu, China, where she is currently working toward the Ph.D. degree with the School of Optoelectronic Science and Engineering. Her research interests include mode-locking optoelectronic oscillator and microwave photonic radar.

Yilin Wu received the B.S. degree from the University of Electronic Science and Technology of China, Chengdu, China, in 2022. His research interests include optoelectronic oscillator modeling and mode-locking optoelectronic oscillator.

Zhenwei Fu's biography is not available at the time of publication.

Weiqiang Lyu's biography is not available at the time of publication.

Yali Zhang's biography is not available at the time of publication.

Zhiyao Zhang's biography is not available at the time of publication.

Shangjian Zhang (Member, IEEE) biography is not available at the time of publication.

Heping Li's biography is not available at the time of publication.

Yong Liu's biography is not available at the time of publication.